QM/MM Study of Human Transketolase: Thiamine Diphosphate Activation Mechanism and Complete Catalytic Cycle

Lionel Nauton, Laurence Hecquet, Vincent Théry

QM/MM Study of Human Transketolase: Thiamin Diphosphate Activation Mechanism and Complete Catalytic Cycle

Lionel Nauton[1], *Laurence Hecquet*[1*], *and Vincent Théry*[1*]

[1] Université Clermont Auvergne, CNRS, Clermont Auvergne INP, ICCF, F-63000 CLERMONT-FERRAND, FRANCE.

AUTHOR EMAIL ADDRESS:

Lionel.Nauton@uca.fr ; Laurence.Hecquet@uca.fr ; Vincent.Thery@uca.fr

Abstract: A computational model for Human transketolase was proposed showing that thiamine diphosphate activation was based on His110 in place of His481 reported in yeast TK. In addition, a complete catalytic reaction pathway was investigated using D-ylulose-5-phosphate and D-ribose-5-phosphate as substrates showing at every step a perfect superimposition of our model with high resolution crystallographic structures 3MOS, 4KXV and 4KXX. This study shows that H2N4' of the active thiamine diphosphate "V form" no longer has a self-activating role but also allows self-stabilization of the cofactor and of the Breslow intermediate. These advances in our knowledge of the Human transketolase mechanism offer interesting prospects for the design of new drugs, this enzyme being involved in several diseases, and for a better understanding of the reactions catalyzed by transketolases from other sources.

Introduction

Thiamine diphosphate (ThDP)-dependent enzymes catalyze a wide variety of enzymatic reactions including the formation or cleavage of carbon-sulfur, carbon-oxygen, carbon-nitrogen, and carbon-carbon bonds.[1-4] These properties are of great interest for the chemoenzymatic synthesis of various compounds.[5-8] In this family of enzymes, transketolases (TK, EC 2.2.1.1) (see Scheme S1 in SI) have been largely used, particularly for obtaining enantio-pure sugars and ketoses by stereoselective carboligation.[9,10] For these purposes, TKs from spinach,[11,12] maize,[13] *Saccharomyces cerevisae*,[14-17] *Escherichia coli*,[18-20] and more recently from thermophilic microorganisms such as *Geobacillus stearothermophilus*[21,22] were characterized, in some cases improved by mutagenesis, and used in biocatalysis. TKs from *Plasmodium falciparum* (malaria),[23] *Mycobacterium tuberculosis* (tuberculosis)[24] and humans[25] were identified and studied for novel therapeutic approaches.

All TKs require the same cofactor ThDP (see Scheme S2 in SI) and display a very similar active site based on five key histidine residues, His30, His69, His103, His263, and His481 (yeast numbering), except for HuTK, in which histidine in the 481 position is replaced by glutamine. The influence of this change on the catalytic mechanism HuTK could offer new perspectives in structure-based drug design[26-28] to find new ways to obtain high specificity, especially for malaria and tuberculosis treatments. In addition, other recent studies have shown that HuTK is potentially involved in other health disorders such as various cancers, diabetes or Alzheimer's disease.[29,30]

The mechanism of ThDP-dependent enzymes has been extensively studied using different spectroscopic techniques conducted on various enzymes of this protein family.[31-35] ThDP

activation is the initial, crucial reaction common to all ThDP-dependent enzymes, and has been the subject of controversy over the past thirty years, as related in several recent publications (see Scheme S3 in SI).[36 39]

In the past decade, high-resolution three-dimensional structures of HuTK have been determined, in the presence of different natural substrates, revealing[25] high homologies with the yeast TK active site.[40.]

Based on the previous work of Breslow[41], Sable & Meschke,[42] Schneider *et al.*[43] and Meyer *et al*,[44] we propose[45] a new activation of the ThDP mechanism in yeast TK involving His481 as the final acceptor of the C2 ThDP proton with the help of a water molecule bridge.[44,46] This single-step activation occurs with a Gibbs free energy of activation of only 9.33 kJ.mol^{-1}. Unlike the previous studies, we showed that H2N4'of the active ThDP in the "V form" no longer has a self-activating role but also allows self-stabilization of the cofactor (Figure 1).

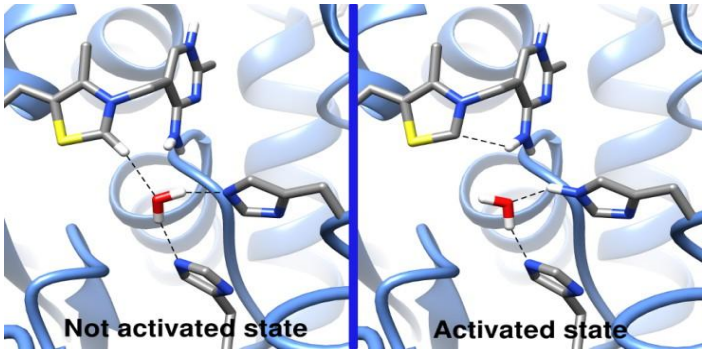

Figure 1. Concerted ThDP activation mechanism in the yeast TK active site.[40]

On the basis of crystallographic HuTK structures available in the PDB (3MOS, 4KXV, 4KXX)[25,40] we propose a computational model for HuTK using a QM/MM method. This model shows that ThDP activation in HuTK is based on His110, confirming our previous hypothesis with yeast TK concerning the possible involvement of His103A in the ThDP activation

mechanism. In addition, we describe the complete catalytic reaction pathway of HuTK in the enzyme environment and using D-xylulose-5-phosphate (DX5P) and D-ribose-5-phosphate (DR5P) as substrates (Scheme 1).

Materials and Methods

Computational strategy

All computations were performed with GAUSSIAN 09 rev D03[47] using the two-layer ONIOM[48,49] method with mechanical and electronic embedding. For the "LOW" layer, the Amber force field[50] was used. For the "HIGH" layer, the density functional theory (DFT)[51,52] level with B3LYP[53-56] hybrid functional and 6-31G basis (see SI of Ref 45) sets were applied. Energy minimizations were performed with the Quadmac[57] option. Every section between the high and the low layer was defined on a σ bond.

All the results (ThDP activation and complete reaction path) were obtained with the following protocol. Starting from the initial minimized structure, an energy scan was performed by stretching a chosen bond. All these energy profiles had a maximum corresponding to a geometry from which a transition state (TS) optimization calculation was performed. Each TS was then validated by the intrinsic reaction coordinate (IRC). Both structures obtained after twenty or more points in forward and reverse directions were minimized at the B3LYP/6-31G level, taking into account thermochemistry corrections at 298.15 K and 1.0 atm. IRC-reactant and IRC-product were respectively obtained. A frequency calculation was done to check the minima and the transition state.

Design of the model using a two-layer ONIOM method for the activation mechanism

The model was designed from the A chain of the HuTK 3MOS[25] structure. HuTK as yeast TK are functional as dimers. The structure resulting from high resolution crystallographic data was a monomer, so the construction of the dimeric TK structures was therefore necessary. The hydrogens were automatically added. All residues were thus protonated automatically except for His residues, which were manually protonated depending on their abilities to form a hydrogen bond with their immediate surroundings. His37A, His77A and His110A of the active site were thus protonated on Nδ and on Nε for His258A. Glu160A and Glu366B were also manually protonated and set in their neutral form because they directly interact with each other and N1' of ThDP. The model was built from a sphere of 20 Å centered on C2 ThDP including every amino acid involved in ThDP activation or stabilization. The following amino-acids were included, A Chain: Leu22A to Phe52A, Phe71A to Trp86A, Leu97A to Met135A, Tyr150A to Met167A, Ala180A to Arg205A, Gly218A to Hid219A, Ile238A to Pro263A, Gln367A to Val374A, Thr394A to Glu407A and for the B chain: Gly161B to Tyr173B, Ala316B to Leu325B, Ala337B to Ala373B, Phe385B to Ile400B, Asn411B to Phe437B, Phe469B to Glu476B, Asp561B to Tyr563B, Val592B to Leu601B. All free amines (N-terminal) and free carboxylic acids (C-terminal) of each polypeptide chains were set in their ionic form. Finally, the model contained 5146 atoms including crystallographic water molecules, and the total charge is equal to -3.

The "HIGH" layer (Figure 2, green sticks) contained 164 atoms including the ThDP cofactor, without the ethyl-pyrophosphate group, and the side chains for His37A, His77A, Arg101A, His110A, His258A, Ser427B and Gln428B. The sequence OGly123A-Ser124A-NLeu125A, making hydrogen bonds with ThDP N4'H and N3' respectively was also added. The sequence CAGlu423B-Asp424B-CAgly425A was added, the carboxylic groups from Glu160A[58], Glu366B[59,60] and the water molecules (3MOS crystallographic number) H_2O26A (HOH661.A),

H_2O29A (HOH659.A), H_2O196A (HOH770.A), H_2O233A (HOH875.A), H_2O511A (HOH840.A) and H_2O775A (HOH934.A) were also included. This HIGH layer was extended to Glu160A, known to play an important role in proton transfers given the significant decrease in activity on mutation of this residue. There were no frozen atoms in this layer and the total charge is equal to -1.

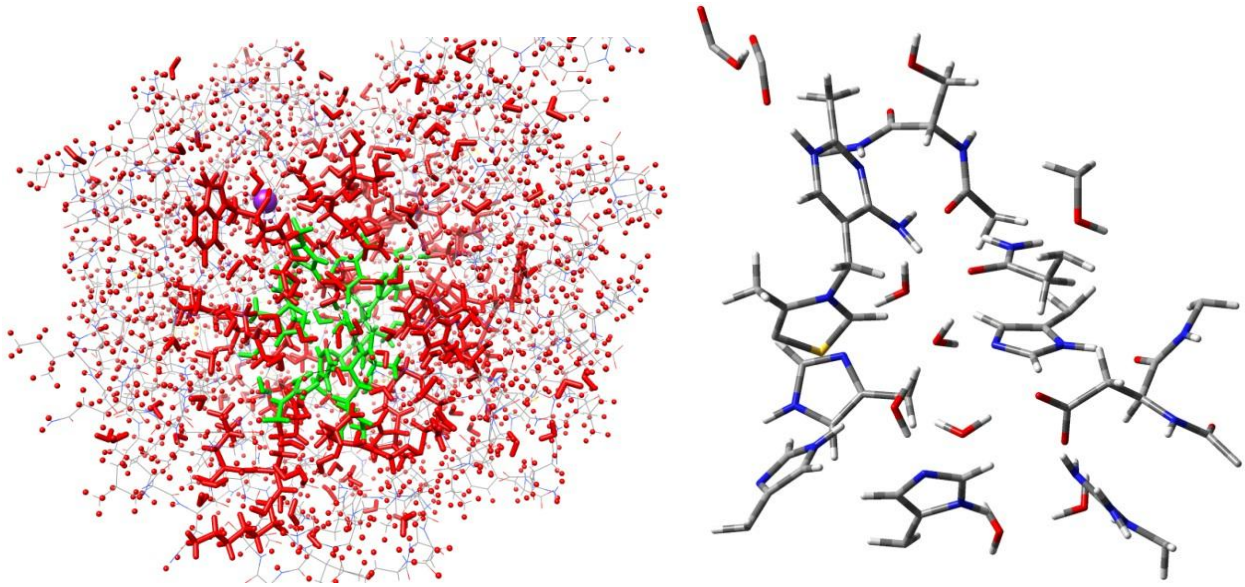

Figure 2. Left: QM/MM system: high layer (green stick), low layer free atoms (red stick), and low layer frozen atoms (wire). Right: High layer details of activation mechanism stage with 164 atoms.

The "LOW" layer was divided into two parts. The first part containing 2979 atoms was free during energy minimization, especially all the hydrogens of the protein (Figure 2, red sticks) whereas the second one (2003 atoms Figure 2, wire) was frozen. The low layer atoms at the periphery of our model system were frozen. The unfrozen part contained all the amino acids surrounding the high layer, the ethyl-pyrophosphate group and 151 water molecules (Gaussian Input file in SI). The atoms included in the HIGH layer and those from the first part of the LOW

layer were defined iteratively until the result of the geometry optimization came as close as possible to the X-ray diffraction data (XRD).

Design of the model using a two-layer ONIOM method for acyl-enzyme formation

Our acyl-enzyme formation model was slightly different from the activation mechanism model and was designed from the HuTK 4KXV[40] sub-ångström-resolution crystallographic structure, owing to the addition of DX5P and the removal of water molecules occupying the same space in the activation model. This model thus contained a total of 5142 atoms with 182 free atoms in the "HIGH" layer, and 4960 atoms in the "LOW" layer of which 1839 were frozen (see Gaussian input file in SI).

Design of the model using a two-layer ONIOM method for D-sedoheptulose-7-phosphate formation

The last step model was once again different from the two previous models and was designed from the HuTK 4KXX[40], also a sub-ångström-resolution crystallographic structure in the presence of the donor ketose phosphate, D-sedoheptulose-7-phosphate (DS7P). This model contained a total of 5247 atoms with 199 free atoms in the "HIGH" layer, and 5048 atoms in the "LOW" layer, of which 1925 were frozen (see Gaussian input file in SI).

Results and Discussion

Description of the ThDP initial state

We focused on the hydrogen bond network in the vicinity of ThDP C2 (Figure 3) consistent with crystallographic data (Figure 4A). The first optimized geometry at the B3LYP/6-31G level

showed a short hydrogen bond (Table 1, entry 1m) reflecting a strong interaction between H_2O196A and His110A, together with a lower but still strong interaction with OE2-Gln428B (Table 1, entry 2m) (Figure 4A). In addition, H_2O196A was also involved in a hydrogen bond with the ThDP-C2 proton (Table 1, entry 4m). These results indicate a putative role of this water molecule in ThDP deprotonation as a bridge between C2 and Nε of His110A.

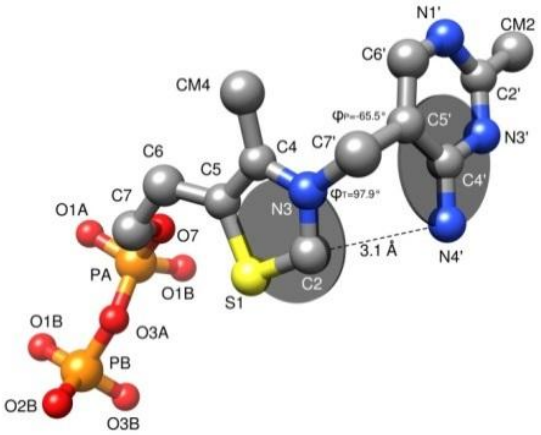

Figure 3. Atom numbering of the ThDP. The same nomenclature is used throughout this work.

Glu366B was initially protonated, but after minimization, the proton was spontaneously transferred and assigned to N1′ of ThDP (Table 1, entry 11m) inducing a mesomeric effect in the pyrimidine cycle. The short C4′-N4′ distance (Table 1, entry 9m) clearly indicated a π delocalization towards an N4′ state close to sp2 hybridization (Table 1, entry 4m) corresponding to an iminium group. Interestingly, the HN4′ proton interacted *via* a hydrogen bond with OE1Gln428B (Table 1, entry 6m), and not with H2O196A as reported with yeast TK. The NE2Gln428B interacted with OGly123A and OGSer427B.

Reaction pathway: **ThDP activation**

From this first minimized structural model, we investigated the reaction pathway (Scheme 1) by stretching the C2-H bond.

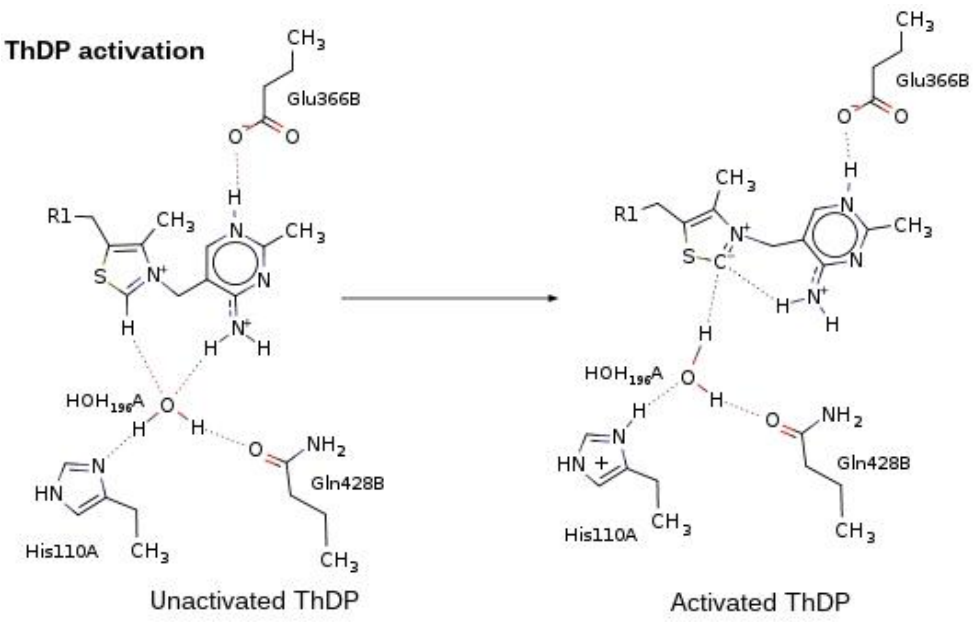

Scheme 1. Overview of ThDP activation

The scan gave a presumed transition state (TS) (Figure 4 B, transition state) corresponding to a C2-H bond distance of 1.124 Å. IRC-reactant (Figure 4 A, inactivated ThDP) and IRC-product (Figure 4 C, activated ThDP) were respectively obtained. A comparison of bond lengths and angle values obtained in the model (Table 1 and Table 2, entry m) and in the IRC reactant (Table 1 and Table 2, entry a) revealed no significant differences, validating our model.

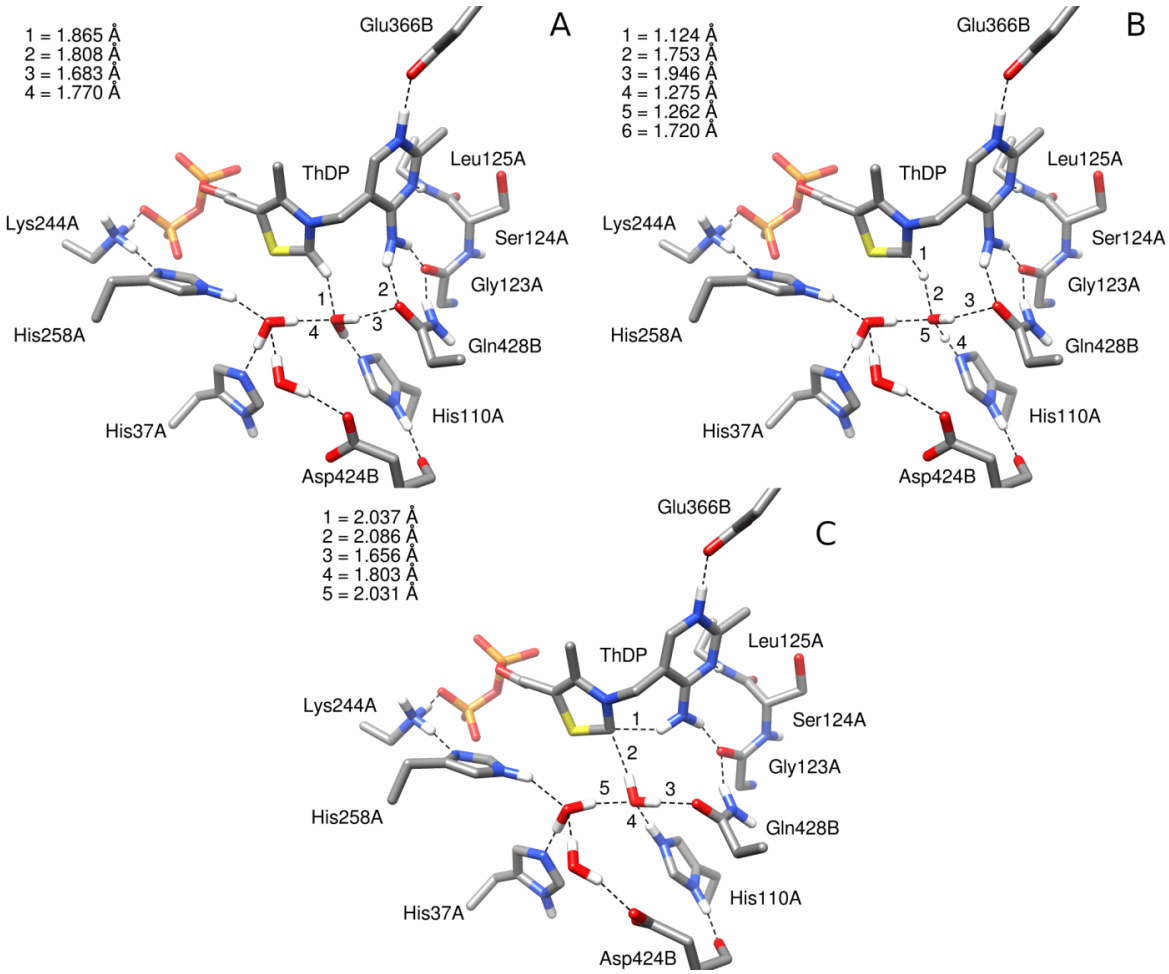

Figure 4. IRC-Reactant **a** (**A**), Transition State **b** (**B**) and IRC-product **c** (**C**) of ThDP activation mechanism.

Table 1. Distances between the targeted atoms in HuTK active site after geometry optimization at B3LYP/6-31G level.

Entry	Bond type	Bond length (Å)			
		Initial model(**m**)	IRC reactant (**a**)	Transition state (**b**)	IRC product (**c**)
1	HOH(196A)-NE2-His110.A	1.682	1.682	1.275	1.039
2	HOH(196A)-OE1-Gln428B	1.808	1.808	1.947	1.656
3	C2-H	1.101	1.100	1.124	2.087
4	C2H-OH2(196A)	1.864	1.865	1.753	0.991
5	HO-H(196A)	1.040	1.039	1.263	1.803
6	N4'H-OE1 Gln428B	1.920	1.920	1.915	3.393
7	N4'H-C2	3.075	3.074	3.046	2.037
8	N4'-C2	3.306	3.305	3.296	2.941

9	C4'-N4'	1.334	1.334	1.332	1.334
10	H-OGlu366B	1.544	1.544	1.561	1.540
11	N1'-HOGlu366B	1.069	1.069	1.065	1.066
12	N1'-OGlu366B	2.607	2.607	2.622	2.593
13	C2-NE2-His110A	5.272	5.272	5.096	5.511

Table 2. Bond angles between the targeted atoms in the HuTK active site after geometry optimization at the B3LYP/6-31G level

Entry	Angle type	Bond angle (Å)			
		Initial model(**m**)	IRC reactant (**a**)	Transition state (**b**)	IRC product (**c**)
1	HO-H(196A)-NE2-His110A	165.26	165.26	168.66	158.13
2	HO-H(196A)-OE1-Gln428B	153.47	153.44	148.68	166.92
3	C2-H-OH(196A)	152.46	152.47	155.29	157.03
4	H-N4'-H	113.47	113.49	113.87	120.10
5	N4'-H-C2	93.72	93.73	94.77	145.91
6	N4'-H-OE1-Gln428B	153.91	153.88	152.44	127.90
5	C4'-N4'-H	125.56	125.56	125.35	119.95
7	C2-O(196A)- NE_His110A	141.38	141.45	145.23	142.61
8	N4'-O(196A)- NE2-His(110A)	104.12	104.17	104.86	108.81

As described in our previous work on yeast TK, we found a ThDP activation mechanism that consisted in removal of the proton carried by C2 *via* a water molecule and the transfer of the proton to a histidine. As expected, His110 was a proton-accepting base and may explain the change of His481 in yeast TK into Gln428 in HuTK, which cannot accept a proton. The HN4′ interacted with OE1 of Gln428B and no longer with a water molecule. As a result, the water molecule H2O196A was somewhat distant from HN4'. The structural role of ThDP was unchanged and offered a self-stabilization of the carbene by the iminium group of ThDP. We superimposed with MatchMaker module of UCSF Chimera[61] software each of the three structures (IRC-Reactant, TS and IRC-Product) with the 3MOS crystallographic structure. We determined the distances between each ThDP atoms in 3MOS and in the models corresponding

to the three steps (Figure S1-S3 in SI). We found that the proposed ThDP activated structure came closest to the average structure described by the XRD.

Regarding the system's energy, the slight difference between DFT and ONIOM energy on the TS (6.4 kJ.mol^{-1}, SI : Table S2) showed a good correlation between the calculation level (B3LYP/6-31G energy and geometry optimization) of the high layer and the atomic coordinates of the whole protein (XRD structure). In addition, the Gibbs free energy value (at 298.15 K, 1 atm) of the TS (−3.8 kJ.mol^{-1}, 9.66 kJ.mol^{-1} yeast TK) obtained with the present ThDP activation pathway suggests that the ThDP activation in HuTK could be spontaneous and not go through a TS. Hence ThDP may be directly activated as soon as the dimerization of the enzyme occurs.

This ThDP activated computational structure came very close to the HuTK crystallographic structure 3MOS[25] and was based on the deprotonated C2 ThDP allowing no distortion of the ThDP thiazole ring. However, we noted that some high resolutions of TK structures are not compatible with the common geometry of a thiazole ring.[38]

In addition, the HuTK and yeast TK computational structures showed slight differences. Taking into account the Gibbs free energy of the TS (−3.8 kJ.mol^{-1}, SI :Table S2), the IRC-Reactant (**a**) cannot be detected or isolated. This result is a first difference from the activation mechanism of ThDP in yeast TK in which the TS energy value was +9.4 kJ.mol^{-1}, showing that the reactant can be isolated.[2,33-35] The second difference compared to yeast TK, concerned the Gibbs free energy of the IRC-Product (**c**), corresponding to the activated state (−69.06 kJ.mol^{-1} in HuTK against −17.41 kJ.mol^{-1} in yeast TK) showing a very strong stabilization of the ThDP carbene in HuTK.

These thermodynamic investigations on ThDP activation considering the TK environment support our proposed mechanism, although we observed previous differences between HuTK

and yeast ThDP activation. These could be due to the presence of His481 in HuTK replaced by a Gln in yeast TK and also to the partial atomic charges of each low layer (Universal Force Field: UFF for yeast TK and Amber for Human TK). Recently[39] a QM/MM study of the self activation model obtained with high level Ab-initio methods (DLPNO-CCSD(T)), wide basis set (6-311+G(2d,2p), aug-cc-pVDZ and aug-cc-pVTZ) and an energy extrapolation scheme (CBS) gives a TS Gibbs free energy of 5.1 Kcal.mol^{-1} (+21.3 kJ.mol-1 vs -3.8 kJ.mol-1 for the self-stabilization model). We can note that in this work the chemical system involved the 4'-iminopyrimidine and not the 4'-aminopyrimidine and did not take into account the amino-imino tautomerism.

Reaction pathway: from activated ThDP with D-**xylulose-5-phosphate (DX5P) as donor substrate to acyl-enzyme (first stage)**

To study the first stage (Scheme 2) of the biochemical reaction, we started from the structure 4KXV[40] in which the donor substrate DX5P reacted with the activated ThDP form. This intermediate can be expected to shift towards the formation of the acyl-enzyme "Breslow intermediate" by cleaving the C9 and C10 bond of DX5P (Figure 5), or conversely, return to the ThDP activated form and the linear form of DX5P. At this stage, we noted a major difference between the 4KXV and 3MOS structures in the orientation of the side chain of the Gln428B. Two scans were performed with the model obtained from the structure 4KXV. The first one was obtained by stretching the bond between C2 of ThDP and C9 of DX5P. Under these conditions, DX5P was found to be in an interaction with the activated ThDP. The second scan was done by stretching the bond between C9 and C10 of DX5P (Figure 5) and led to the formation of the acyl-enzyme (Breslow intermediate BI) and the release of glyceraldehyde-3-phosphate (DG3P).

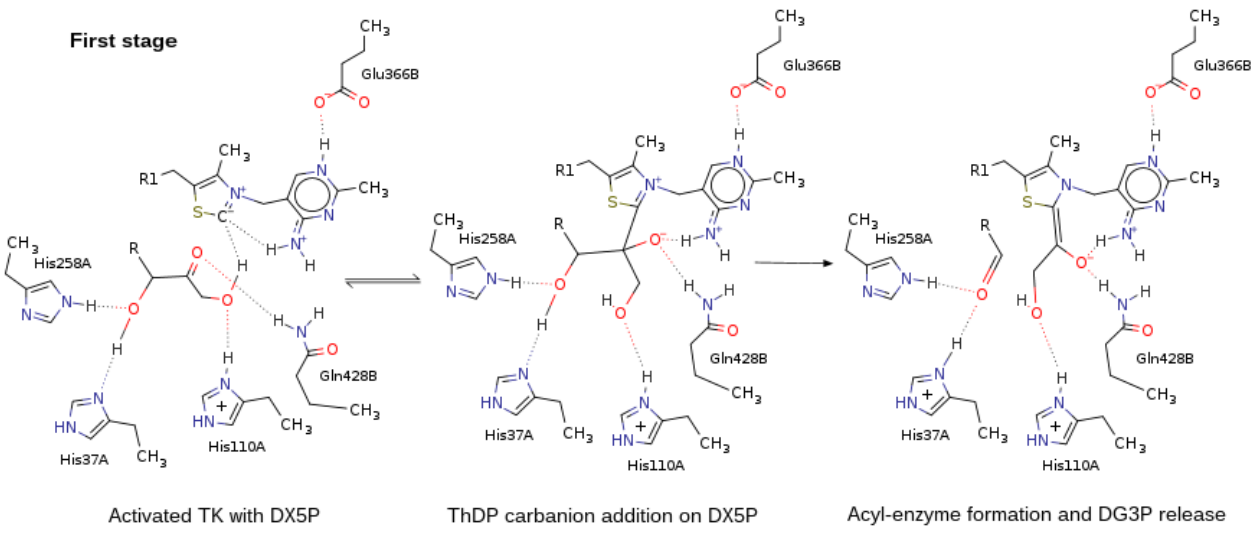

Scheme 2. Overview of first stage of the proposed TK catalytic mechanism

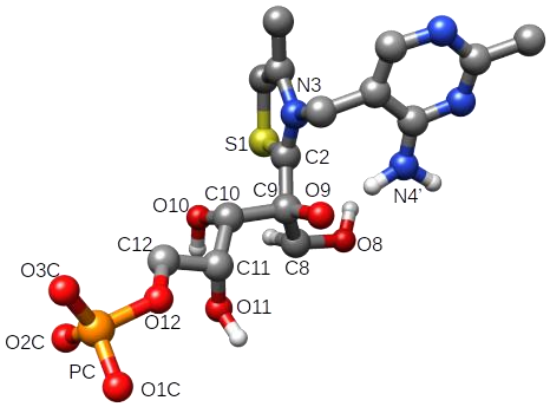

Figure 5. Atom numbering of ThDP in the two steps of the first stage

First step of the first stage: acyl-enzyme formation

The interaction of DX5P with the activated ThDP required Gln428B different rotations, 55° (149° to −156°) around the CA-CB bond, −148° (72° to −76°) around the CB-CG bond and −76° (22° to −54°) around the CG-CD bond. These conformational changes were induced by DX5P, which drove the water molecule H_2O196A (yellow oxygen position in Figure 6A) towards the back of the site.

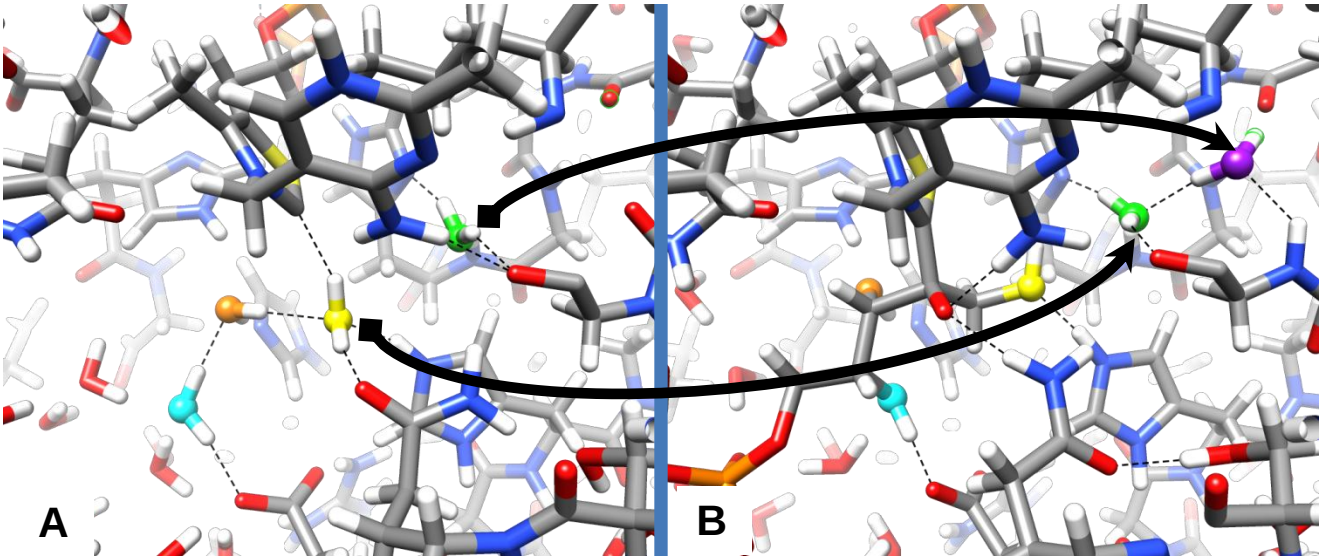

Figure 6. Displacement of water molecules between 3MOS (A) and 4KXV (B) due to the entry of DX5P. The oxygen positions are colored in yellow, green, purple, cyan and orange.

The movement of the water molecule H_2O196A caused the amide function to rotate around the CG-CD axis and the nitrogen to replace the oxygen position. A hydrogen bond was thus formed between HNE2 Gln428B and the O9 oxygen of the carbonyl group (Figure 6, B). The oxygen O8 (yellow oxygen position in Figure 6 B) of DX5P can interact with the C2 of ThDP acting as a hydrogen bond donor and with the His110A acting as a hydrogen bond acceptor (Figure 7 A). These interactions were the direct consequences of the His110A protonation due to the ThDP activation step. When O8 oxygen replaced H_2O196A, this water molecule can be pushed into a pocket behind the site. We had already investigated this water molecule storage area in the yeast TK, but the lower resolution of its three-dimensional structure did not support this hypothesis. In HuTK, this process appeared more clearly.

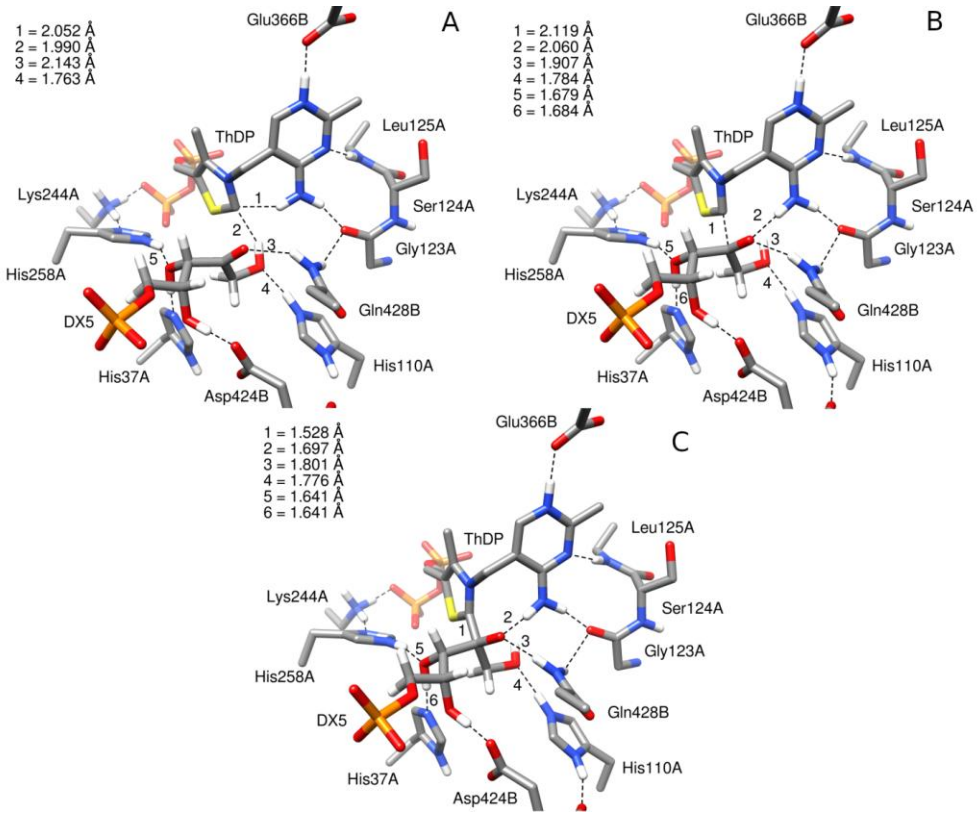

Figure 7. IRC reactant a_1 (A), transition state b_1 (B) and IRC product c_1 (C) of DX5P addition mechanism

The molecule expected to be responsible for ThDP activation (yellow oxygen position in the Figure 6A) could be pushed by the head of DX5P to firstly adopt the positions of HOH 875 in 3MOS or HOH 7102 in the structure 4KXV (green oxygen position in Figure 6). The water molecule HOH 875 in 3MOS was in turn pushed to the bottom of the pocket to take the position of HOH 7181 in the structure 4KXV (purple oxygen position in Figure 6). This cascading movement towards the bottom of the pocket may be responsible for the backbone flip of Thr122 carbonyl oxygen that was in direct interaction with the water molecule network, which in turn stabilized the rotation of the Gln428 side chain (Figure 6) Although neither our calculations nor crystallography data can yet prove the expected sequence of events, we note that the enzyme structure plasticity allowed the energy levels to be decreased at all stages of this process.

The HO10 hydroxyl (Figure 5) interacted with His258A acting as hydrogen bond acceptor and His37A acting as a hydrogen bond donor (Figure 7A). Once again, the oxygen O10 of DX5P was in the same position as HOH840 in 3MOS in the ThDP activations step (orange oxygen position in Figure 6). The HO11 hydroxyl of DX5P also replaced HOH770 in 3MOS and interacted with Asp424A acting as a hydrogen bond acceptor (cyan oxygen position in Figure 6)

The phosphate moiety of DX5P interacted directly with Arg318B and Arg474B, and indirectly with Lys260A *via* a water molecule. The value of the angle formed by the thiazolium ring and the DX5P carbonyl function (O9-C9-C10-C8) was 56.5 ° and the distance between ThDP C2 and DX5P C9 was 3.04 Å. In the transition state (Figure 7B), these planes have an angle of 76.6° and the distance between ThDP C2 and DX5P C9 was 2.119 Å (Table 3, entry $1b_1$). The DX5P C9 was in an intermediate state between sp2 and sp3 and was slightly pyramidized (O9-C9-C10 angle equal to 118.2°). The interaction of HN4′ ThDP with C2-ThDP was transferred to DX5P O9 carbonyl oxygen (Table 3, entry $9b_1$-$10b_1$), and the interaction between HO8 hydroxyl and C2 ThDP disappeared (Table 3, entry $4b_1$). The other interactions previously described for HO10 an HO11 remained identical.

The IRC product (**c_1**) formed from TS (**b_1**) (Figure 7), has the same structure as that observed in the 4KXV structure (Figure S4-S9 in SI). The DX5P C9 has a sp3 structure, and the distance between ThDP C2 and DX5P C9 was 1.528 Å (Table 3, entry $1c_1$) The DX5P O9 oxygen gave a functional group closer to an alcoholate than to a carbonyl group (Table 3, entry $5c_1$), which could form a very strong hydrogen bond with HN4' (Table 3, entry $9c_1$) and with HNE1 of the Gln428B (Table 3, entry $11c_1$). In this step, the carbene / iminium ion interaction became an alcoholate / iminium ion interaction helping to stabilize the reaction intermediate. The other interactions described in the TS structure remained identical.

Table 3. Distance between targeted atoms during the reaction of activated HuTK on DX5P (atom nomenclature in Figure 5).

Entry	Bond type	Bond length (Å)		
		IRC reactant **(a_1)**	Transition state **(b_1)**	IRC product **(c_1)**
1	$C2_{ThDP}$-$C9_{DX5P}$	3.040	**2.119**	**1.528**
2	$C2_{ThDP}$-$N3_{ThDP}$	1.355	1.351	1.348
3	$C2_{ThDP}$-$S1_{ThDP}$	1.789	1.775	1.769
4	$C2_{ThDP}$-$HO8_{DX5P}$	1.989	**2.487**	**2.887**
5	$C9_{DX5P}$-$O9_{DX5P}$	1.249	1.295	1.398
6	$C9_{DX5P}$-$C10_{DX5P}$	1.525	1.557	**1.642**
7	$N\varepsilon_{His37}$-$HO10_{DX5P}$	1.653	1.682	1.640
8	$O10_{DX5P}$-$HN\varepsilon_{His258A}$	1.746	1.678	1.642
9	$HN4'_{ThDP}$-$O9_{DX5P}$	3.155	**2.060**	**1.696**
10	$HN4'_{ThDP}$-$C2_{ThDP}$	2.052	**2.649**	**2.669**
11	$HN_{Gln428B}$-$O9_{DX5P}$	2.142	1.908	**1.801**
12	H-$O10_{DX5P}$	1.027	1.026	1.035

At this stage, an early TS (**b_1**) appeared, and its energy was due to the covalent bond formation between the DX5P carbonyl group and the ThDP C2. The release of the carbene by HN4' allowed the simultaneous creation of an interaction with DX5P O9 (Table 3, entry 8-9), but without proton transfers as previously reported in the literature.[29,30,32] These modifications also induced a reorientation of the C2 thiazole ring toward DX5P (Table 3, entry 1). These new interactions were reinforced in the IRC product, and $C2_{ThDP}$-$C9_{DX5P}$ bond was formed and $C9_{DX5P}$-$O9_{DX5P}$ bond was modified after the TS. This observation appeared as a difference from the usual pattern described in the literature in which a hypothetical acid HB2[14] or HN4'[32,33] could help in the formation of the reaction intermediate. The TS energy was high +50.1 kJ and the product (**c_1**) was somewhat destabilized by the environment as shown by its low energy (+8.3 kJ) (SI: Table S3).

We note that the distance of the C9-C10 DX5P bond (1.64 Å) was already weakened in the product (**c_1**) (1.613 Å in 4KXV and 1.629 Å in 4KXX). We also observed that the energy of the TS (**b_1**) was of the same order as the stabilization energy of the activated ThDP.

Second step of the first stage: release of D-glyceraldehyde-3P (DG3P)

During this second step, the IRC reactant (Figure 8a) corresponded to the IRC product of the first step. (DFT energy difference = 0.01 kJ.mol^{-1}). The stretching of the C9-C10 bond of DX5P (Table 4, entry 6) spontaneously induced proton transfer from the C10 hydroxyl of DX5P to His37A (Table 4, entry 7) and not to His258A as mentioned by Prejanò *et al*.[36,37] We opted to protonate Nε of His258A assuming that Lys244A was in its charged form, due to its direct interaction with the pyrophosphate group. It was unlikely that Lys244A was in the NH2 form, by being linked to a pyrophosphate group. The pKa of lysine could be reinforced by this interaction, and the exchange of lysine proton with His258 Nδ may be very unfavorable. The direct interaction between Lys244 and His258Nδ did not allow protonation of Nε by another route. The His258Nε nitrogen was accessible to the solvent and permanently protonated. The double bond between ThDP C2 and DX5P C9 was initiated (Table 4 entry 1c_2).

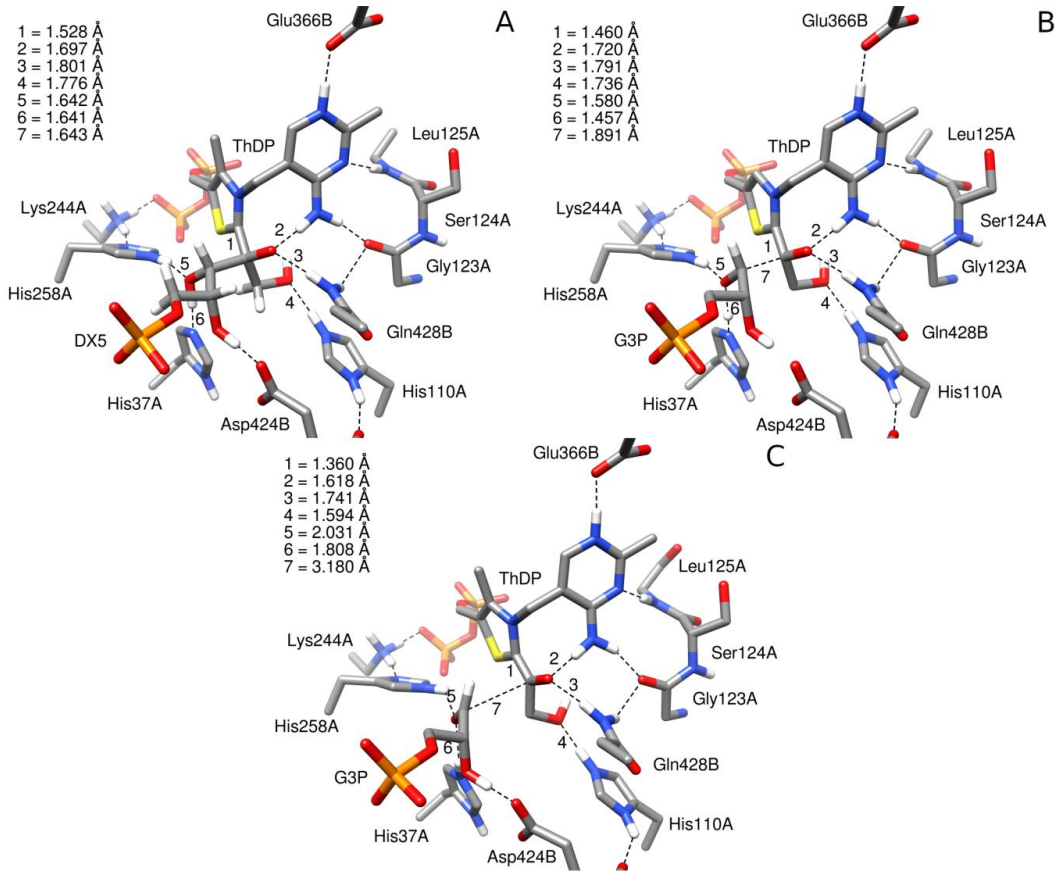

Figure 8. IRC reactant a_2 (A), transition state b_2 (B) and IRC product c_2 (C) of acyl-enzyme formation and DG3P release

On the TS (Figure 8B) (imaginary frequency −194.42 *i* cm^{-1}) we observed a slight modification of interaction *vs.* IRC-Reactant. In the IRC product (**c_2**) a new interaction between the O8 oxygen of DX5P and His77A was established *via* a water molecule (H_2O103). The other interactions remained unchanged. The structure of the acyl-enzyme in HuTK (Figure 8C) differed from the Breslow intermediate described in yeast TK by the non-protonation of O9 from the carbonyl group of DX5P from the first step. In addition, the stabilization of the enolate was ensured by HN4′ of ThDP (Table 4, entry $9c_2$) and HNE1 of Gln428B (Table 4, entry $11c_2$).

From an energy point of view, the TS energy (9.3 kJ) was low and the product particularly well-stabilized by the environment (−68.4 kJ) (SI: Table S4). Figure 9 shows the complete energy profile of the reaction of the donor substrate with HuTK, showing that the limiting step is the binding between the ThDP and the substrate.

Table 4. Distance between the targeted atoms during acyl-enzyme "Breslow intermediate" (BI) formation.

Entry	Bond type	Bond length (Å)		
		IRC reactant **(a_2)**	Transition state **(b_2)**	IRC product **(c_2)**
1	$C2_{ThDP}$-$C9_{DX5P}$	1.528	**1.460**	**1.360**
2	$C2_{ThDP}$-$N3_{ThDP}$	1.348	1.367	1.428
3	$C2_{ThDP}$-$S1_{ThDP}$	1.769	1.787	1.850
4	$C2_{ThDP}$-$HO8_{DX5P}$	2.887	2.859	3.247
5	$C9_{DX5P}$-$O9_{DX5P}$	1.398	1.385	1.367
6	$C9_{DX5P}$-$C10_{DX5P}$	**1.642**	**1.891**	**3.180**
7	$N\varepsilon_{His37}$-$HO10_{DX5P}$	1.640	**1.112**	1.037
8	$O10_{DX5P}$-$HN\varepsilon_{His258A}$	1.642	1.579	**2.031**
9	$HN4'_{ThDP}$-$O9_{DX5P}$	1.696	1.720	1.617
10	$HN4'_{ThDP}$-$C2_{ThDP}$	2.669	2.649	2.658
11	$HN_{Gln426B}$-$O9_{DX5P}$	1.801	1.791	1.741
12	H-$O10_{DX5P}$	1.035	**1.458**	**1.808**

We cannot compare the full profile with that obtained by Prejanò in HuTK.[36,37] because the reaction pathway was not the same. Obviously, proton transfer between O10, His258A and Lys244A seemed unfavorable. The proximity of Lys244A to the pyrophosphate group of ThDP required His258A protonation not in the Nδ position but in Nε. Furthermore, the energy of the acyl-enzyme in our model could prevent going backwards by a strong stabilization of the Breslow intermediate (figure 9). This last point is not contradictory with the 4KVX structure which is equivalent of the state c1/a2 in our model giving an energy of 68.4 kJ.mol-1 higher than

that obtained for the acyl enzyme. Indeed, the 4KVX structure is the most stable state under the conditions of the crystallographic experiments. Our model corresponds to the physiological conditions of the enzyme, i.e. without the constraints due to the crystallographic stacking and the presence of cryoprotectants that restrict the conformational changes of the enzyme. These conformational changes are necessary to reach the acyl enzyme and to ensure the release of Glyceraldehyde-3-P which were not observed in 4KVX.

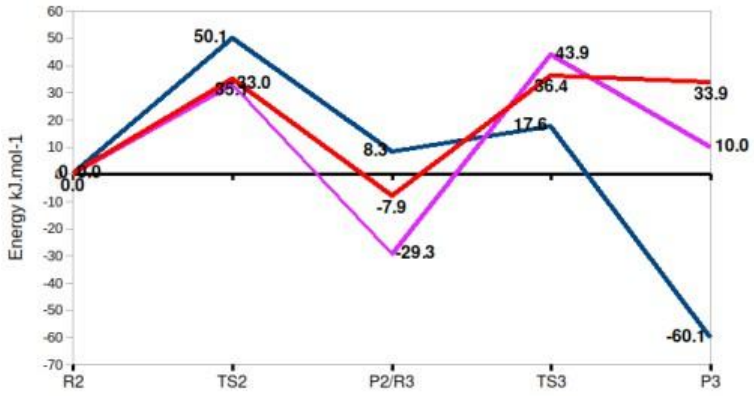

Figure 9. Profile of Free Gibbs energy (kJ.mol^{-1}) of the acyl enzyme formation "Breslow intermediate". R2, TS2 and P2: IRC reactant, TS and IRC product of acyl-enzyme formation. R3, TS3 and P3: IRC reactant, TS and IRC product of DG3P release step. Blue curve this work. Red curve Prejano *et al.*,[36] Magenta curve Prejano *et al*.[37]

Reaction pathway: **from acyl-enzyme with** D**-ribose-5-phosphate (DR5P) as acceptor substrate to the product (second stage)**

To study this second stage of the TK-catalyzed reaction (Scheme 3), we started from the structure 4KXX in which HuTK was co-crystalized with D-sedoheptulose-7-phosphate (DS7P) as donor. We used this structure as the result of the reaction of the acyl-enzyme with the acceptor DR5P. Two scans were performed. The first one was by stretching the bond between C9 and C10

(Figure 10) of DS7P considered as the product of the reaction between DR5P and the acyl-enzyme. The second scan was done by stretching the bond between the ThDP C2 and DS7P C9 (Figure 10) and led to the release of the regenerated ThDP and of DS7P.

First step of the second stage: addition of acyl-enzyme on DR5P

The oxygen O10 (Figure 10) of DR5P formed two hydrogen bonds, the first with His37A protonated in DG3P release step and the second with His258ANε in neutral form (Figure 11A and Table 5, entry $7a_3$-$8a_3$). DR5P hydroxyl HO11 formed a hydrogen bond with Asp424B. The phosphate group was stabilized by hydrogen bonds with His416B, Arg318B, Arg474B, Ser345B and interacted through a water molecule with Lys260A. Intramolecular hydrogen bonds were formed in DR5P between hydroxyl HO12 and phosphate and between hydroxyl HO13 and O10 oxygen of the aldehyde function. The two planes defined by the two sp2 carbons C9 (BI) and C10 (DR5P) were almost parallel (angle values 13.4°)

In the TS (**b_3**) (Figure 11B), clearly characterized by an imaginary frequency of −180.70 *i* cm^{-1}, the formation of the C9-C10 bond, the proton transfer from Hip37A to O10 and the elongation of the O10-C10 bond were observed. The other interactions found in IRC reactant remained identical.

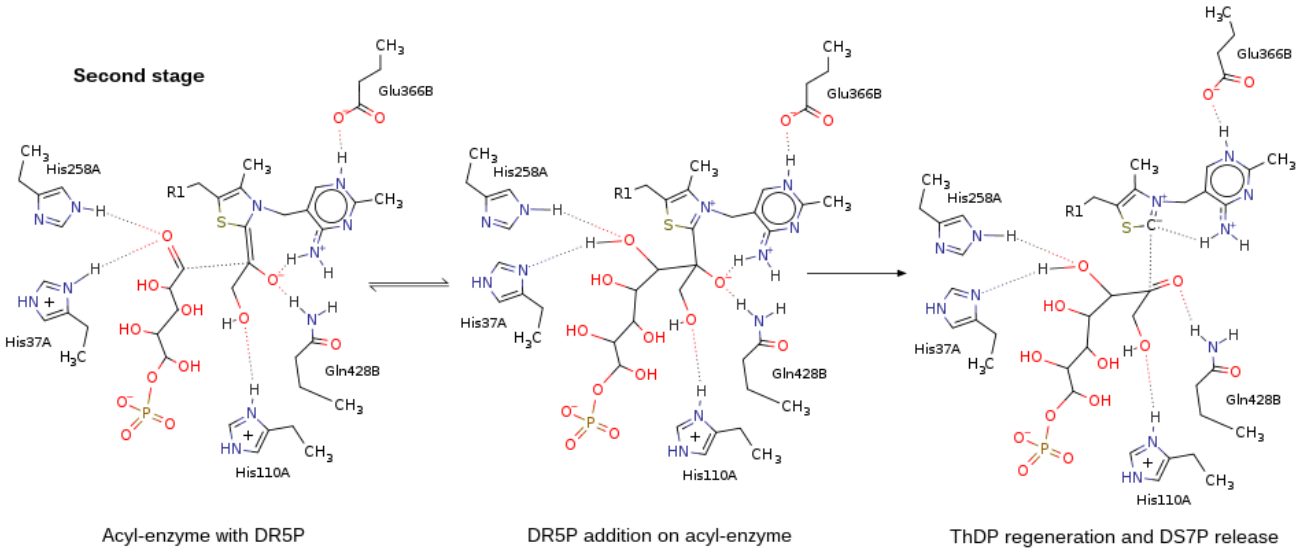

Scheme 3. Overview of the second stages of the proposed TK catalytic mechanism.

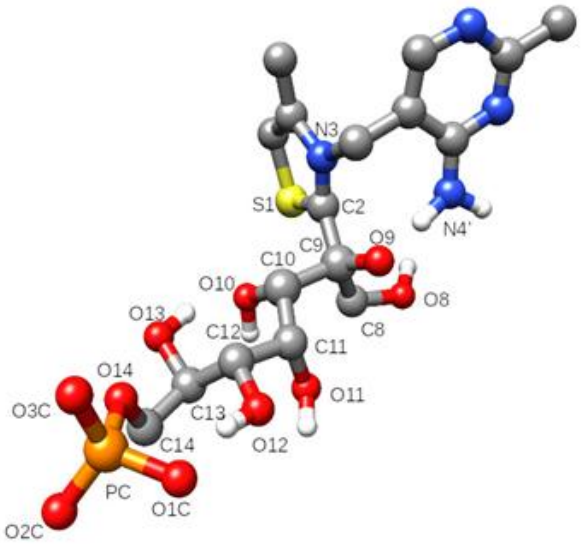

Figure 10. Atom numbering of ThDP for both steps of the second stage.

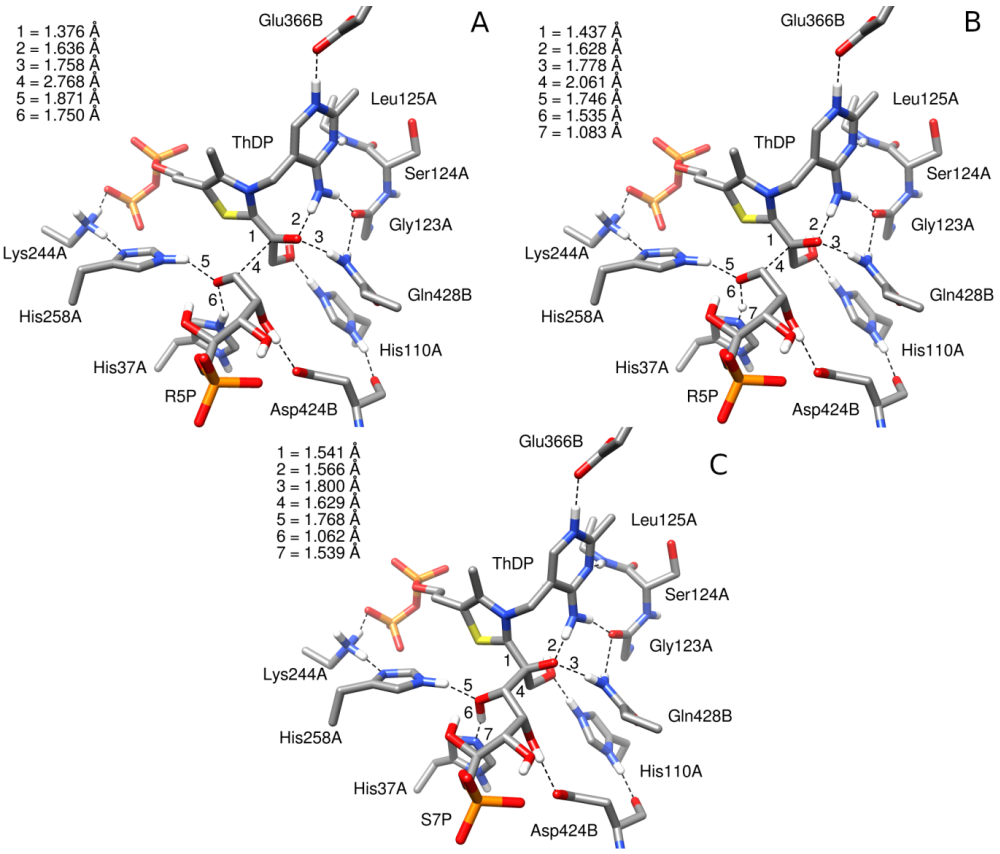

Figure 11..IRC reactant $\mathbf{a_3}$ (A), Transition State $\mathbf{b_3}$ (B) and IRC product $\mathbf{c_3}$ (C) of DR5P addition mechanism.

Table 5. Distance between targeted atoms during reaction of the DR5P on acyl-enzyme "Breslow intermediate" (BI).

Entry	Bond type	Bond length (Å)		
		IRC reactant **($\mathbf{a_3}$)**	Transition state **($\mathbf{b_3}$)**	IRC product **($\mathbf{c_3}$)**
1	$C2_{ThDP}$-$C9_{BI}$	1.375	**1.437**	**1.541**
2	$C2_{ThDP}$-$N3_{ThDP}$	1.419	1.381	1.346
3	$C2_{ThDP}$-$S1_{ThDP}$	1.838	1.798	1.765
4	$C2_{ThDP}$-$HO8_{BI}$	3.297	3.282	3.342
5	$C9_{BI}$-$O9_{BI}$	1.366	1.371	1.396
6	$C9_{BI}$-$C10_{DR5P}$	2.768	**2.061**	**1.629**
7	$HN\varepsilon_{Hip37}$-$O10_{DR5P}$	1.750	**1.534**	1.062
8	$O10_{DR5P}$-$HN\varepsilon_{His258A}$	1.872	1.746	1.768
9	$HN4'_{ThDP}$-$O9_{BI}$	1.636	1.627	1.567
10	$HN4'_{ThDP}$-$C2_{ThDP}$	2.634	2.621	2.631
11	$HN_{Gln428B}$-$O9_{BI}$	1.758	1.778	1.800
12	C10-O10	1.268	**1.339**	**1.446**

After the TS, the IRC product (Figure 11C) had the same structure as that observed in 4KXX (see Figure S10-S15 in SI). These results highlighted an incomplete formation of the C9-C10 bond as shown by its length (1.629 Å) (Table 5, entry $6c_3$). We note that in the 4KXX crystallographic structure, the value of this bond was 1.673 Å, close to that obtained in our study. The other interactions found in IRC reactant remained identical.

Second step of the second stage: ThDP regeneration and release of DS7P product

During this final step, the IR reactant (**a_4**) (Figure 12A) was the IRC product (**c_3**) (Figure 11C) of the previous step (addition of acyl-enzyme on the DR5P carbonyl group). All the values corresponding to the two structures were identical, though obtained from two different scan calculations (DFT energy difference 0.25 kJ). The stretching of the C2-C9 bond gave a TS (Table 6, entry $1b_4$) characterized by an imaginary frequency of −184.59 *i* cm^{-1} and led to the ketone function and the C9-C10 σ bond formation.

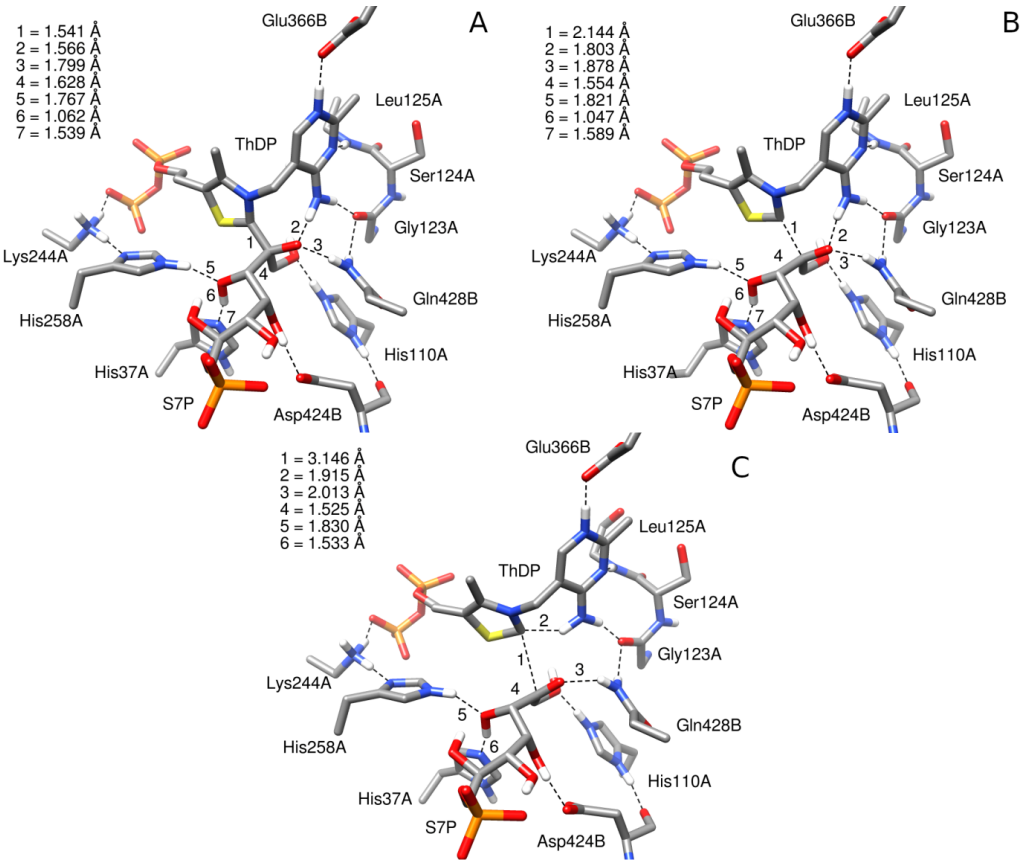

Figure 12. IRC reactant $\mathbf{a_4}$ (A), Transition State $\mathbf{b_4}$ (B) and IRC product c $_4$ (C) of ThDP regeneration and DS7P.

Table 6. Distance between targeted atoms during the ThDP regeneration step and DS7P formation.

Entry	Bond type	Bond length (Å)		
		IRC reactant **(a_4)**	Transition state **(b_4)**	IRC product **(c_4)**
1	$C2_{ThDP}$-C9	1.541	**2.144**	**3.146**
2	$C2_{ThDP}$-$N3_{ThDP}$	1.347	1.347	1.350
3	$C2_{ThDP}$-$S1_{ThDP}$	1.766	1.773	1.787
4	$C2_{ThDP}$-HO8	3.342	3.259	2.959
5	C9-O9	1.396	**1.294**	**1.248**
6	C9-C10	1.628	**1.554**	**1.525**
7	$HN\varepsilon_{Hip37}$-O10	1.062	1.046	1.059
8	O10 -$HN\varepsilon_{His258A}$	1.767	1.822	1.829
9	$HN4'_{ThDP}$-O9	1.566	**1.803**	**2.790**
10	$HN4'_{ThDP}$-$C2_{ThDP}$	2.631	2.577	**1.914**
11	$HN_{Gln428B}$-O9	1.800	1.877	**2.013**
12	C10-O10	1.446	1.451	1.448

The stabilized interaction between NH4′ and O9 disappeared after the TS (Table 6, entry $9b_4$-$9c_4$) and simultaneously restoring the interaction between HN4′ and the carbene (Table 6, entry $10b_4$-$10c_4$). The DS7P was then released outside the active site.

The complete energy profile of the reaction with HuTK acyl-enzyme (Table S6 and Figure 13) showed that the limiting step was the release of DS7P. The effective stabilization of the IRC-product (−14.63 kJ.mol-1) due to carbene/iminium interaction prevented a step backwards.

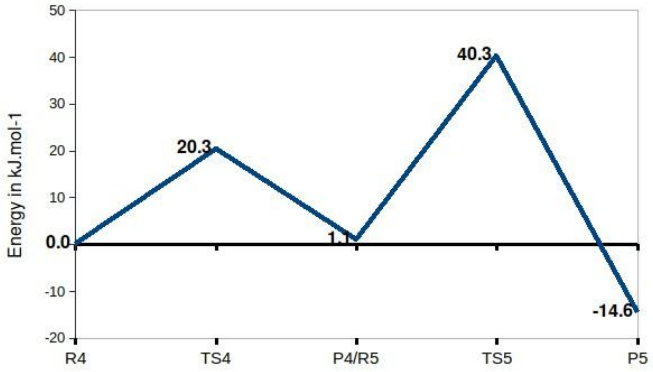

Figure 13. Profile of Free Gibbs energy (kJ.mol^{-1}) from acyl-enzyme to product stage. R4, TS4 and P4: IRC reactant, TS and IRC product of addition of acyl-enzyme on DR5P step. R5, TS5 and P5: IRC reactant, TS and IRC product of ThDP regeneration and release of DS7P step

Conclusions

In this study, we propose a ThDP activation mechanism in HuTK based on His110A (equivalent to His103A in yeast TK) which was the final acceptor of the ThDP C2 proton. In addition, we show that Gln428B (equivalent to His481 in yeast TK) could act as a hydrogen bond acceptor during ThDP activation and after this step could become a hydrogen-bond donor to stabilize the donor substrate (DX5P). The carbene formed was stabilized by the iminium function on the

nitrogen N4′ of ThDP showing a self-stabilization of ThDP and no longer a role of self-activation as described till now. The energy profile shows our model to be more compatible than that published based on the yeast TK mechanism and shows a "spontaneous" activation of ThDP in HuTK. We also propose a new structure for the acyl-enzyme “Breslow intermediate” with an enolate self-stabilized by ThDP through the iminium function on N4'. Proton exchange was no longer needed to form the acyl enzyme in contrast to the current mechanism described in the literature. We show that the energy profile of our model is more compatible with HuTK enzymatic kinetics than the energy profiles given in the literature with HuTK

The superimposition of our three model atomic co-ordinates (for activated ThDP, acyl-enzyme and regenerated ThDP formation) with those of the three corresponding XRD structures (3MOS, 4KXX and 4KXV respectively) show a very high similarity (distances < 0.2Å) and let us propose a plausible HuTK reaction sequence. The energy profiles show that ThDP activates and acyl-enzyme are well-stabilized and that the reverse pathway is higher-energy (+79 $kJ.mol^{-1}$) than the forward reaction (+50 $kJ.mol^{-1}$), preventing a step backwards.

We observed the same activation mechanism in yeast TK and in HuTK with two different histidine positions. This ThDP activation mechanism could be applied to other histidine positions around ThDP in TK from various sources if one or two water molecules can create a proton pathway between the ThDP C2 and a histidine.

These advances in the understanding of the HuTK reaction mechanism offer interesting perspectives in the design of new drugs for the treatment of diseases in which HuTK is involved. Our findings can also be used to gain better knowledge of the catalytic mechanisms of TKs from other sources sources used for biocatalytic applications.

Data and Software Availability

All crystallographic structures 3MOS, 4KXV and 4KXX are available on Protein Data Bank (PDB). The preparation of the PDB structures was done with UCSF Chimera 1.12. All computations were performed with GAUSSIAN 09 rev D03. The protocols were detailed in the section "Computational strategy". All finals results are available in supporting information (Gaussian input format files with ONIOM two-layer setting). All superpositions were made with MatchMaker module of UCSF Chimera.[5]

ASSOCIATED CONTENT

Supporting Information.

All model 3D structures as Gaussian input format file with ONIOM calc (ZIP)

Summary of the TK reaction mechanism and the ThDP activation mechanism in the literature (PDF)

ThDP parameters for Amber force field (PDF)

All superimposed structures between our models and XRD Structures 3MOS, 4KXV and 4KXX (PDF)

AUTHOR INFORMATION

Corresponding Authors

Vincent.Thery@uca.fr

Laurence.Hecquet@uca.fr

Notes

The authors declare they have no competing financial interest.

ACKNOWLEDGMENTS

Computations were performed on the facilities of "Mésocentre" at the University Clermont Auvergne. The authors thank Prof. P. Hoggan for fruitful discussions.

ABBREVIATIONS

TK, transketolase; HuTK, human transketolase; ThDP, thiamine diphosphate; DX5P, D-xylulose-5-phospahte; DR5P, D-ribose-5-phosphate; DS7P, D-sedoheptulose-7-phosphate; BI, Breslow intermediate

REFERENCES

1. Schellenberger, A. Sixty Years of Thiamin Diphosphate Biochemistry, *BBA Protein Struct. M.* **1998***, 1385*, 177–186.

2. Jordan, F. Original Mechanistic Understanding of Thiamin Diphosphate-dependent enzymatic reactions, *Nat. Prod. Rep.* **2003***, 20*, 184–201.

3. Frank, R. A. W., Leeper, F. J., Luisi, B. F. Structure, Mechanism and Catalytic Duality of Thiamine-Dependent Enzymes, *Cell. Mol. Life Sci.* **2007***, 64*, 892–905.

4. Pohl, M., Sprenger, G. A., Müller, M. A New Perspective on Thiamine Catalysis, *Curr. Opin. Biotech.* **2004***, 15*, 335–342.

5. Enders, D., Niemeier, O., Henseler, A. Organocatalysis by N-heterocyclic Carbenes*, Chem Rev.* **2007***, 107*, 5606–5655.

6. Zeitler, K. Extending Mechanistic Routes in Heterazolium Catalysis – Promising Concepts for Versatile Synthetic Methods, *Angew. Chem. Int. Edit.* **2005***, 44*, 7506–7510.

7. Demir, A. S., Ayhan, P., Sopaci, S. B. Thiamine Pyrophosphate Dependent Enzyme Catalyzed Reactions: Stereoselective C–C Bond Formations in Water, *CLEAN – Soil, Air, Water.* **2007***, 35,* 406–412.

8. Müller, M., Gocke, D., Pohl, M. Thiamin Diphosphate in Biological Chemistry: Exploitation of Diverse Thiamin Diphosphate-Dependent Enzymes for Asymmetric Chemoenzymatic Synthesis, *FEBS J.* **2009***, 276*, 2894–2904.

9. Kobori, Y., Myles, D. C., Whitesides, G. M. Substrate Specificity and Carbohydrate Synthesis Using Transketolase. *J. Org. Chem.* **1992***, 57*, 5899-5907.

10. Turner, N. J. Applications of Transketolases in Organic Synthesis. *Curr. Opin. Biotechnol.* **2000***, 11*, 527–531.

11. Flechner, A., Dressen, U., Westhoff., P., Henze, K., Schnarrenberger, C., Martin, W. Molecular Characterization of Transketolase (EC 2.2.1.1) Active in the Calvin Cycle of Spinach Chloroplasts. *Plant Mol. Biol.* **1996***, 32*, 475 –484.

12. Demuynck, C., Bolte, J., Hecquet, L., Dalmas, V. Enzyme-Catalyzed Synthesis of Carbohydrates: Dynthetic Potential of Transketolase, *Tetrahedron Lett.* **1991***, 32*, 5085–5088.

13. Gerhardt, S., Echt, S., Busch, M., Freigang, J., Auerbach, G., Bader, G., F. Martin, W.F., Bacher, A., Huber, R., Fischer, M. Structure and Properties of an Engineered Transketolase from Maize. *Plant Physiol.* **2003***, 132*, 1941–1949.

14. Wikner, C., Nilsson, U., Meshalkina, L., Udekwu, C., Lindqvist, Y., Schneider, G. Identification of Catalytically Important Residues in Yeast Transketolase. *Biochemistry* **1997***, 36*, 15643−15649.

15. Lindqvist, Y., Schneider, G., Ermler, U., Sundstrom M. Three-Dimensional Structure of Transketolase, a Thiamine Diphosphate Dependent Enzyme, at 2.5 A Resolution. *EMBO J.* **1992***, 11*, 2373 –2379.

16. Schneider, G., Lindqvist, Y. Crystallography and Mutagenesis of Transketolase: Mechanistic Implications for Enzymatic Thiamin Catalysis. *Biochim. Biophys. Acta* **1998***, 1385*, 387–398.

17. Benaissi, K., Hélaine, V., Prévot, V., Forano, C., Hecquet, L. Efficient ImmoBIization of Yeast Transketolase on Layered Double Hydroxides and Application for Ketose Synthesis, *Adv. Synth. Catal.* **2011***, 353*, 1497–1509.

18. Sprenger, G.A., Schorken, U., Sprenger, G., Sahm, H. Transketolase A of Escherichia coli K12. Purification and Properties of the Enzyme from Recombinant Strains. *Eur. J. Biochem.* **1995***, 230*, 525–532.

19. Ingram, C. U., Bommer, M., Smith, M. E., Dalby, P. A., Ward, J. M., Hailes, H. C., Lye, G. J. One-Pot Synthesis of Amino-Alcohols Using a de-Novo Transketolase and β-Alanine: Pyruvate Transaminase Pathway in Escherichia Coli, *Biotechnol. Bioeng.* **2007***, 96*, 559–569.

20. Subrizi, F., Cárdenas-Fernández, M., Lye, G. J., Ward, J. M., Dalby, P. A., Sheppard, T. D., Hailes, H. C. Transketolase Catalysed Upgrading of L-Arabinose: The One-Step Stereoselective Synthesis of l-Gluco-Heptulose. *Green Chem.* **2016***, 18*, 3158-3165.

21. Abdoul Zabar, J., Lorillière, M., Yi, D. Nauton, L., Charmantray, F., Hélaine, V., Fessner, W.D., Hecquet, L. Engineering a Thermostable Transketolase for Unnatural Conversion of (2S)-Hydroxyaldehyde. *Adv. Synth. Catal.* **2015***, 357*, 1715-1720.

22. Lorillière, M., Dumoulin, R., L'Enfant, M., Rambourdin, A., Thery, V., Nauton, L., Fessner, W.-D., Charmantray, F., Hecquet, L. Evolved Thermostable Transketolase for Stereoselective Two-Carbon Elongation of Non-Phosphorylated Aldoses to Naturally Rare Ketoses. *ACS Catal.* **2019***, 9*, 4754-4763.

23. Joshi, S., Singh A.R., Kumar, A., Misra, P.C., Siddiqi, M.I., Saxena, J.K. Molecular Cloning and Characterization of Plasmodium Falciparum Transketolase. *Mol. Biochem. Parasitol.* **2008***, 160*, 32–41.

24. Fullam, E., Pojer, F., Bergfors, T., Jones, T.A, Cole S.T. Structure and Function of the Transketolase from Mycobacterium Tuberculosis and Comparison with the Human Enzyme. *Open Biol.* **2011***, 2*, 110026. http://dx.doi.org/10.1098/rsob.110026.

25. Mitschke, L., Parthier, C., Schröder-Tittmann, K., Coy, J., Lüdtke, S., Tittmann, K. The Crystal Structure of Human Transketolase and New Insights into Its Mode of Action, *J. Biol. Chem.* **2010***, 285*, 31559 –31570.

26. Zhao, J., Zhong, C.-J. A Review on Research Progress of Transketolase, *Neurosci. Bull.* **2009***, 25*, 94–99.

27. Le Huerou, Y., Gunawardana, I., Thomas, A. A., Boyd, S. A., de Meese, J., Dewolf, W., Gonzales, S. S., Han, M., Hayter, L., Kaplan, T., Lemieux, C., Lee, P., Pheneger, J., Poch, G.,

Romoff, T. T., Sullivan, F., Weiler, S., Wright, S. K., Lin, J. Prodrug Thiamine Analogs as Inhibitors of the Enzyme Transketolase, *Bioorg. Med. Chem. Lett.* **2008***, 18*, 505–508.

28. Thomas, A. A., De Meese, J., Le Huerou, Y., Boyd, S. A., Romoff, T. T., Gonzales, S. S., Gunawardana, I., Kaplan, T., Sullivan, F., Condroski, K., Lyssikatos, J. P., Aicher, T. D., Ballard, J., Bernat, B., DeWolf, W., Han, M., Lemieux, C., Smith, D., Weiler, S., Wright, S. K., Vigers, G., Brandhuber, B. Non-Charged Thiamine Analogs as Inhibitors of Enzyme Transketolase, *Bioorg. Med. Chem. Lett.* **2008***, 18*, 509–512.

29. Butterworth, R. F. Thiamin in Shils, M. E. Modern Nutrition In *Health And Disease.* (Lippincott Williams & Wilkins, ed.) 10th ed., Lexington Books, Boston. **2006**, 23, 426-434.

30. Gibson, G.E., Hirsch, J.A., Cirio, R.T, Jordan, B.D., Fonzetti, P., Elder, J. Abnormal Thiamine-Dependent Processes in Alzheimer's Disease. Lessons from Diabetes. *Mol Cell Neurosci.* **2013***, 55*, 17–25. doi:10.1016/j.mcn.2012.09.001.

31. Duggleby, R. G. Domain Relationships in Thiamine Diphosphate-Dependent Enzymes, *Acc. Chem. Res.* **2006***, 39*, 550–557.

32. Wang, J. J., Martin, P. R., Singleton, C. K. Aspartate 155 of Human Transketolase is Essential for Thiamine Diphosphate-Magnesium Binding, and Cofactor Binding is Required for Dimer Formation, *Biochim. Biophys. Acta* **1997***, 1341*, 165–172.

33. Balakrishnan, A., Gao, Y., Moorjani, P., Nemeria, N.S., Tittmann, K., Jordan, F. Bifunctionality of the Thiamin Diphosphate Cofactor: Assignment of Tautomeric/Ionization States of the 4′-Aminopyrimidine Ring When Various Intermediates Occupy the Active Sites

during the Catalysis of Yeast Pyruvate Decarboxylase *J. Am. Chem. Soc.* **2012**,.*134 (8),* 3873–3885.

34. Balakrishnan, A., Paramasivam, S., Chakraborty, S., Polenova, T., Jordan, F. Solid-State Nuclear Magnetic Resonance Studies Delineate the Role of the Protein in Activation of Both Aromatic Rings of Thiamin: *J. Am. Chem. Soc.* **2012***, 134*, 665–672.

35. Chakraborty, S., Nemeria, N. S., Balakrishnan, A., Brandt, G. S, Kneen, M. M., Yep, A., McLeish, M. J., Kenyon, G. L., Petsko, G. A., Ringe, D. Jordan, F. Detection and Time Course of Formation of Major Thiamin Diphosphate-Bound Covalent Intermediates Derived from a Chromophoric Substrate Analogue on Benzoylformate Decarboxylase. *Biochemistry* **2009***, 48,* 981–994.

36. Prejanò, M., Estefan,y Medina F., Fernandes, P.A., Russo, N., Ramos, M.J., Marino T. The Catalytic Mechanism of Human Transketolase. *ChemPhysChem.* **2019***, 20*, 1-7.

37. Prejano, M., Medina, F.E., Ramos, M.J., Russo, N., Fernandes, P.A., Marino, T. How the Destabilization of a Reaction Intermediate Affect Enzymatic efficiency/ The Case of Human Transketolase. ACS *Catal.*. **2020***, 10*, 2872-2881.

38. Hsu, N.S.Wang,Y.-W., Lin, K.-H. Liu, Y.C., Chang, C.Y., Wu, C.J., Li, T.L. The Mesomeric Effect of Thiazolium on non-Kekulé Diradicals in Pichia Stipitis Transketolase. *Angew. Chem. Int. Ed.* **2018***, 57*, 1802-1807.

39. Medina, F.E, Prejano, M. Water Molecules Allow the Intramolecular Activation of the Thiamine Di-Phosphate Cofactor in Human TransKetolase: Mechanistic Insights into a Famous Proposal. ACS *Catal.* **2021***, 11*, 4136-4145

40. Ludtke, S., Neumann, P., Erixon, K.M., Leeper, F., Kluger, R., Ficner, R., Tittmann, K. Sub-Angstrom-Resolution Crystallography Reveals Physical Distortions that Enhance Reactivity of a Covalent Enzymatic Intermediate. *Nat. Chem.* **2013***, 5*, 762-767.

41. Breslow, R. The Mechanism of Thiamine Action: Predictions from Model Experiments, *Ann. N.-Y. Acad. Sci.* **1962***, 98*, 445–452.

42. Sable, H.Z. Meschke, D.J. Studies on the Mechanism of Catalysis by Thiamin: Progress and Problems in *Catalysis in chemistry and biochemistry theory and experiment*. (B. Pullman ed) **1979** pp113-123

43. Schneider, G., Sundström, M., Lindqvist, Y. Preliminary Crystallographic Data for Transketolase from Yeast, *J. Biol. Chem.* **1989***, 264*, 21619–21620.

44. Meyer, D., Neumann, P., Ficner, R. Tittmann, K. Observation of Stable Carbene at the Active Site of a Thiamine Enzyme. *Nat. Chem. Biol.* **2013***, 9*,488-490.

45. Nauton, L., Helaine, V., Thery, V. Hecquet, L. Insights into the Thiamine Diphosphate Enzyme Activation Mechanism: Computational Model for Transketolase Using a Quantum Mechanical/Molecular Mechanical Method. *Biochemistry* **2016***, 55*, 2144−2152.

46. Lie, M.A. Schiøtt, B. A. DFT Study of Solvation Effects on the Tautomeric Equilibrium and Catalytic Ylide Generation of Thiamin Models, *J. Comput. Chem.* **2008***, 29*, 1037–1047.

47. http://www.gaussian.com/g_tech/g_ur/m_citation.htm.

48. Dapprich, S., Komáromi, I., Byun, K. S., Morokuma, K., Frisch M. J. A. New ONIOM Implementation in Gaussian 98. 1. The Calculation of Energies, Gradients and Vibrational Frequencies and Electric Field Derivatives, *J. Mol. Struct. Theochem* **1999***, 461*, 1-21.

49. Vreven, T., Byun, K. S., Komáromi, I., Dapprich, S., Montgomery, J. A., Morokuma, K., Frisch, M. J. Combining Quantum Mechanics Methods with Molecular Mechanics in ONIOM. *J. Chem. Theory and Comput.* **2006***, 2*, 815-826.

50. Cornell, W. D., Cieplak, P., Bayly, C. I., Gould, I. R., Merz K. M., Ferguson, D. M., Spellmeyer, D. C., Fox, T., Caldwell, J. W. Kollman, P. A. A Second-Generation Force-Field for the Simulation of Proteins, Nucleic-Acids, and Organic-Molecules, *J. Am. Chem. Soc.* **1995***, 117*, 5179-5197.

51. Hohenberg, P. Kohn, W. Inhomogeneous Electron Gas. *Phys. Rev.* **1964***, 136*, B864-B871.

52. Kohn, W. Sham, L.J. Self-Consistent Equations Including Exchange and Correlation Effects, *Phys. Rev.* **1965***, 140*, A1133-A38.

53. Becke, A. D. Density-functional Thermochemistry. III. The Role of Exact Exchange, *J. Chem. Phys.* **1993***, 98*, 5648-5652.

54. Lee, C., Yang, W., Parr, R.G. Development of the Colle-Salvetti Correlation-Energy Formula into a Functional of the Electron Density, *Phys. Rev. B* **1988***, 37*, 785-789.

55. Vosko, S. H., Wilk, L., Nusair, M. Accurate Spin-Dependent Electron Liquid Correlation Energies for Local Spin Density Calculations: A Critical Analysis, *Can. J. Phys.* **1980***, 58*, 1200-1211.

56. Stephens, P. J., Devlin, F. J., Frisch, M. J. Chabalowski, C. F. Ab initio Calculation of Vibrational Absorption and Circular Dichroism Spectra Using Density Functional Force Fields, *J. Phys. Chem.* **1994***, 98*, 11623-11627.

57. Vreven, T., Frisch, M. J., Kudin, K. N., Schlegel, H. B., Morokuma, K. Geometry Optimization with QM/MM Methods. II. Explicit Quadratic Coupling, *Mol. Phys.* **2006***, 104*, 701-704.

58. Meshalkina, L., Nilsson, U., Wikner, C., Kostikowa, T., Schneider, G. Examination of the Thiamin Diphosphate Binding Site in Yeast Transketolase by Site-Directed Mutagenesis, *Eur. J. Biochem.* **1997***, 244*, 646–652.

59. Sevostyanova, I., Solovjeva, O., Selivanov, V., Kochetov, G. Half-of-the-Sites Reactivity of Transketolase from Saccharomyces Cerevisiae, *Biochem. Biophys. Res. Commun.* **2009***, 379*, 851–854.

60. Frank, R. A. W. A Molecular Switch and Proton Wire Synchronize the Active Sites in Thiamine Enzymes*, Science* **2004***, 306*, 872–876.

61. UCSF Chimera – A Visualization System for Exploratory Research and Analysis. Pettersen EF, Goddard TD, Huang CC, Couch GS, Greenblatt DM, Meng EC, Ferrin TE. *J. Comput. Chem* **2004**. *13*, 1605-1612.

BRIEFS

Thiamin diphosphate activation mechanism in Human transketolase and new structure for the acyl-enzyme “Breslow intermediate” using D-xylulose-5-phosphate and D-ribose-5-phosphate as substrates.

SYNOPSIS